Search for neutrinoless quadruple-β decay of ^{150}Nd with the NEMO-3 detector

R. Arnold, C. Augier, A.S. Barabash, A. Basharina-Freshville, S. Blondel, S. Blot, M. Bongrand, D. Boursette, V. Brudanin, J. Busto, et al.

Search for Neutrinoless Quadruple-β Decay of ^{150}Nd with the NEMO-3 Detector

R. Arnold,[1] C. Augier,[2] A. S. Barabash,[3] A. Basharina-Freshville,[4] S. Blondel,[2] S. Blot,[5] M. Bongrand,[2] D. Boursette,[2] V. Brudanin,[6,7] J. Busto,[8] A. J. Caffrey,[9] S. Calvez,[2] M. Cascella,[4] C. Cerna,[10] J. P. Cesar,[11] A. Chapon,[12] E. Chauveau,[5] A. Chopra,[4] L. Dawson,[4] D. Duchesneau,[13] D. Durand,[12] V. Egorov,[6] G. Eurin,[2,4] J. J. Evans,[5] L. Fajt,[14] D. Filosofov,[6] R. Flack,[4] X. Garrido,[2] H. Gómez,[2] B. Guillon,[12] P. Guzowski,[5*] R. Hodák,[14] A. Huber,[10] P. Hubert,[10] C. Hugon,[10] S. Jullian,[2] A. Klimenko,[6] O. Kochetov,[6] S. I. Konovalov,[3] V. Kovalenko,[6] D. Lalanne,[2] K. Lang,[11] Y. Lemière,[12] T. Le Noblet,[13] Z. Liptak,[11] X. R. Liu,[4] P. Loaiza,[2] G. Lutter,[10] M. Macko,[15,10] C. Macolino,[2] F. Mamedov,[14] C. Marquet,[10] F. Mauger,[12] B. Morgan,[16] J. Mott,[4] I. Nemchenok,[6] M. Nomachi,[17] F. Nova,[11] F. Nowacki,[1] H. Ohsumi,[18] C. Patrick,[4] R. B. Pahlka,[11] F. Perrot,[10] F. Piquemal,[10,19] P. Povinec,[15] P. Přidal,[14] Y. A. Ramachers,[16] A. Remoto,[13] J. L. Reyss,[20] C. L. Riddle,[9] E. Rukhadze,[14] R. Saakyan,[4] R. Salazar,[11] X. Sarazin,[2] Yu. Shitov,[6,21] L. Simard,[2,22] F. Šimkovic,[15] A. Smetana,[14] K. Smolek,[14] A. Smolnikov,[6] S. Söldner-Rembold,[5] B. Soulé,[10] D. Štefánik,[15] I. Štekl,[14] J. Suhonen,[23] C. S. Sutton,[24] G. Szklarz,[2] J. Thomas,[4] V. Timkin,[6] S. Torre,[4] Vl. I. Tretyak,[25] V. I. Tretyak,[6] V. I. Umatov,[3] I. Vanushin,[3] C. Vilela,[4] V. Vorobel,[26] D. Waters,[4] F. Xie,[4] and A. Žukauskas[26]

(NEMO-3 Collaboration)

[1]*IPHC, ULP, CNRS/IN2P3, F-67037 Strasbourg, France*
[2]*LAL, Université Paris-Sud, CNRS/IN2P3, Université Paris-Saclay, F-91405 Orsay, France*
[3]*NRC "Kurchatov Institute," ITEP, 117218 Moscow, Russia*
[4]*UCL, London WC1E 6BT, United Kingdom*
[5]*University of Manchester, Manchester M13 9PL, United Kingdom*
[6]*JINR, 141980 Dubna, Russia*
[7]*National Research Nuclear University MEPhI, 115409 Moscow, Russia*
[8]*Aix Marseille Université, CNRS, CPPM, F-13288 Marseille, France*
[9]*Idaho National Laboratory, Idaho Falls, Idaho 83415, USA*
[10]*CENBG, Université de Bordeaux, CNRS/IN2P3, F-33175 Gradignan, France*
[11]*University of Texas at Austin, Austin, Texas 78712, USA*
[12]*LPC Caen, ENSICAEN, Université de Caen, CNRS/IN2P3, F-14050 Caen, France*
[13]*LAPP, Université de Savoie, CNRS/IN2P3, F-74941 Annecy-le-Vieux, France*
[14]*Institute of Experimental and Applied Physics, Czech Technical University in Prague, CZ-12800 Prague, Czech Republic*
[15]*FMFI, Comenius University, SK-842 48 Bratislava, Slovakia*
[16]*University of Warwick, Coventry CV4 7AL, United Kingdom*
[17]*Osaka University, 1-1 Machikaneyama Toyonaka, Osaka 560-0043, Japan*
[18]*Saga University, Saga 840-8502, Japan*
[19]*Laboratoire Souterrain de Modane, F-73500 Modane, France*
[20]*LSCE, CNRS, F-91190 Gif-sur-Yvette, France*
[21]*Imperial College London, London SW7 2AZ, United Kingdom*
[22]*Institut Universitaire de France, F-75005 Paris, France*
[23]*Jyväskylä University, FIN-40351 Jyväskylä, Finland*
[24]*MHC, South Hadley, Massachusetts 01075, USA*
[25]*Institute for Nuclear Research, 03028 Kyiv, Ukraine*
[26]*Charles University in Prague, Faculty of Mathematics and Physics, CZ-12116 Prague, Czech Republic*

(Received 25 May 2017; revised manuscript received 19 June 2017; published 24 July 2017)

We report the results of a first experimental search for lepton number violation by four units in the neutrinoless quadruple-β decay of ^{150}Nd using a total exposure of 0.19 kg yr recorded with the NEMO-3 detector at the Modane Underground Laboratory. We find no evidence of this decay and set lower limits on the half-life in the range $T_{1/2} > (1.1\text{–}3.2) \times 10^{21}$ yr at the 90% C.L., depending on the model used for the kinematic distributions of the emitted electrons.

DOI: 10.1103/PhysRevLett.119.041801

In the standard model (SM) of particle physics, leptons are assigned a lepton number of $+1$ and antileptons are assigned -1. All experimental observations thus far are consistent with the assumption that the total lepton number L is conserved in particle interactions (for a review of experimental limits on lepton-number violation, see [1]). However, since this is not due to a fundamental symmetry, there is no reason to assume that L is generally conserved in theories beyond the SM.

Lepton-number-violating processes could be directly linked to the possible Majorana nature of neutrinos. If Majorana mass terms are added to the SM Lagrangian, processes appear that violate L by two units ($\Delta L = 2$) [2]. Searches for $\Delta L = 2$ processes such as neutrinoless double-β ($0\nu2\beta$) decay have, therefore, been the focus of many experiments [3,4].

In this Letter, we present a first search for processes with $\Delta L = 4$, which are allowed even if neutrinos are Dirac fermions and $\Delta L = 2$ processes are forbidden [5]. Models with $\Delta L = 4$ have some power in explaining naturally small Dirac masses of neutrinos [6] and could mediate leptogenesis [7]. The models have also been linked with dark matter candidates [8] and with CP violation in the lepton sector [9]. Processes with $\Delta L = 4$ could also be probed at the Large Hadron Collider (LHC), for example, in the pair production and decay of triplet-Higgs states to four identical charged leptons [10].

An experimental signature of some models with $\Delta L = 4$ would be the neutrinoless quadruple-β ($0\nu4\beta$) decay of a nucleus, $(A, Z) \to (A, Z+4) + 4e^-$, where four electrons are emitted with a total kinetic energy equal to the energy $Q_{4\beta}$ of the nuclear transition. The $0\nu4\beta$ half-life is expected to depend strongly on the unknown mass scale Λ_{NP} of the new $\Delta L = 4$ phenomena [5].

The search for $0\nu4\beta$ decay is experimentally challenging, since only three long-lived isotopes can undergo this decay: ^{136}Xe ($Q_{4\beta} = 0.079$ MeV [11]), ^{96}Zr ($Q_{4\beta} = 0.642$ MeV), and ^{150}Nd, which has the highest $Q_{4\beta}$ value of 2.084 MeV. The NEMO-3 detector contained two of these isotopes, ^{96}Zr and ^{150}Nd. The ^{96}Zr decay has too low a $Q_{4\beta}$ value to be detected with high-enough efficiency in NEMO-3 since low-energy electrons would be absorbed in the source. It could instead be studied using geochemical methods [12]. The value of $Q_{4\beta}$ of the decay $^{150}\mathrm{Nd} \to {}^{150}\mathrm{Gd}$, however, is sufficiently large for four electrons to be observable in the NEMO-3 detector.

We search for $0\nu4\beta$ decay by exploiting the unique ability of the NEMO-3 experiment to reconstruct the kinematics of each final-state electron. In the absence of a more complete theoretical treatment of the kinematics of the decay [13], we test four models of the electron energy distributions, labeled uniform, symmetric, semisymmetric, and antisymmetric. This choice is designed to cover a wide range of models and used to demonstrate that the final result is largely model independent.

The uniform model has all four electron kinetic energies T_i distributed uniformly on the simplex $T_1 + T_2 + T_3 + T_4 = Q_{4\beta}$, with each kinetic energy $T_i > 0$. The decay rates dN for the other three models are distributed according to the differential phase space given by

$$\frac{d^4N}{\prod_{i=1}^{4} dT_i} \propto A_m \delta\left(Q_{4\beta} - \sum_{i=1}^{4} T_i\right) \prod_{i=1}^{4} (T_i + m_e) p_i F(T_i, Z), \tag{1}$$

which is an extension of the $0\nu2\beta$-decay phase space [14]. Here, i labels the electrons, m_e is the electron mass, $p_i = \sqrt{T_i(T_i + 2m_e)}$, and A_m is a model-dependent factor. The Fermi function $F(T, Z) \propto p^{2s-2} e^{\pi u} |\Gamma(s + iu)|^2$ describes the Coulomb attraction between the electrons and the daughter nucleus with atomic number Z. In this function, $s = \sqrt{1 - (\alpha Z)^2}$, $u = \alpha Z(T + m_e)/p$, Γ is the gamma function, and α is the fine-structure constant. The three different phase-space distributions differ by the factors $A_m = (1/2)|\epsilon^{ijkl}| P_{ij} P_{kl}$ that depend on the energy asymmetry of electron pairs represented by P, with ϵ the Levi-Civita symbol. For the symmetric distribution $P_{ij} = P_{kl} = 1$ (both pairs prefer a symmetric energy distribution), the semisymmetric distribution has $P_{ij} = 1$, $P_{kl} = (T_k - T_l)^2$ (one pair tends to be symmetric in energy, the other pair asymmetric), and for the antisymmetric distribution $P_{ij} = (T_i - T_j)^2$, $P_{kl} = (T_k - T_l)^2$ (both pairs prefer to be asymmetric). In all models, each electron angular distribution is generated isotropically.

Since electrons produced in the NEMO-3 source foil must have a minimum energy of $\approx$250 keV to fall into the acceptance of the detector, the efficiency is smaller for models producing more low-energy electrons. We show the electron kinetic energy distributions for the four kinematic models in Fig. 1.

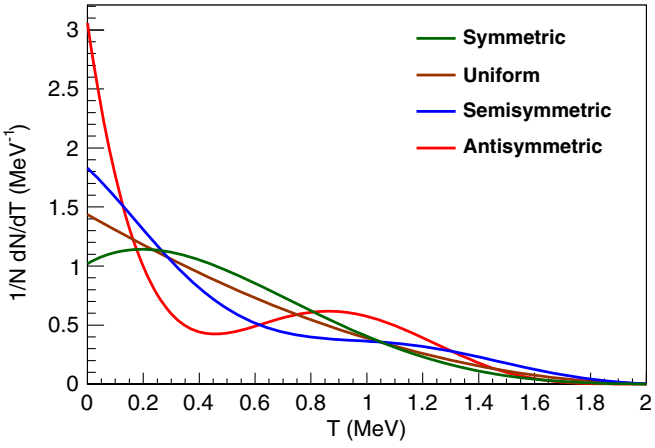

FIG. 1. Normalized distribution of the individual electron kinetic energies T in each $0\nu4\beta$ decay for the four kinematic models.

We perform the search with the NEMO-3 detector on data collected between 2003 and 2011 using 36.6 g of enriched ^{150}Nd source, with a live time of 5.25 yr. The detector is optimized to search for $0\nu2\beta$ decays by reconstructing the full decay topology. It is cylindrical in shape, with the cylinder axis oriented vertically, a height of 3 m, and a diameter of 5 m, and is divided into 20 sectors of equal size. Thin foils with a thickness of 40–60 mg/cm^2 contain seven different isotopes. The Nd foil has a height of 2.34 m and a width of 6.5 cm. The foils are located between two concentric tracking chambers composed of 6180 drift cells operating in Geiger mode. Surrounding the tracking chambers on all sides are calorimeter walls composed of 1940 scintillator blocks coupled to low-activity photomultipliers that provide timing and energy measurements. The calorimeter energy resolution is (14.1–17.7)% (FWHM) at an electron energy of 1 MeV. A vertically oriented magnetic field of ≈25 G allows discrimination between electrons and positrons. Detailed descriptions of the experiment and data sets are given in Refs. [15,16].

In Ref. [17], we describe a measurement of the two-neutrino double-β ($2\nu2\beta$) decay of ^{150}Nd, and provide details of the background model and measured activities that are used in this analysis. The backgrounds are categorized as internal (within the source foil, including contamination of ^{208}Tl and ^{214}Bi), external to the foil (electrons and photons produced in or outside of the detector components), radon diffusion that can deposit background isotopes on the surface of the detector components, and internal contamination in the source foils neighboring the Nd foil, which can have a falsely reconstructed vertex in the Nd foil.

The $0\nu4\beta$ signal selection requires candidate decays that produce three or four tracks originating in the foil. If there are three tracks, all three must be matched to calorimeter hits, which is the signature of a reconstructed electron candidate, while the fourth β electron is assumed to be absorbed in the foil ($3e$ topology). We further distinguish two topologies in the four-track final state, where either all four tracks are associated with calorimeter hits ($4e$ topology) or one of the tracks has no calorimeter hit ($3e1t$ topology).

Internal conversions as well as Møller and Compton scattering are sources of additional electrons in single-β or double-β decays that can mimic three- or four-electron final states. The largest contribution to the background is $2\nu2\beta$ decay of ^{150}Nd to the ground state (g.s.) of ^{150}Sm with a half-life of $T_{1/2} = 9.34 \times 10^{18}$ yr [17]. An additional background source not considered in Ref. [17] is the double-β decay of ^{150}Nd to the 0_1^+ excited state of ^{150}Sm [18], for which we use a half-life of $T_{1/2} = 1.33 \times 10^{20}$ yr [19] in the simulation.

An additional set of selections is applied to all topologies to ensure events are well reconstructed and to reject instrumental backgrounds. Decay vertices in regions of high activity in the foil corresponding to localized contaminations from ^{234m}Pa and ^{207}Bi (hot spots) are rejected. The locations of these hot spots have been determined in Ref. [17]. Events where more than one electron track is associated with the same calorimeter hit are removed. The energy of each associated calorimeter hit must be >150 keV. Events in the $4e$ topology with one associated calorimeter hit below 150 keV are treated as $3e1t$ candidates. The vertical component of the distance between the intersection points of the tracks with the foil must be <8 cm. We apply no requirement in the horizontal direction, since the foil has a width of 6.5 cm. For each event, the track lengths, calorimeter hit times and energies, and their uncertainties, are used to construct two χ^2 values assuming that all tracks originate in the foil (internal hypothesis) or that one track originates outside the foil and scatters in the foil producing secondary tracks (external hypothesis). The probabilities of the internal hypothesis must be >0.1% and of the external hypothesis <4%. Finally, events with unassociated calorimeter hits with energies >150 keV in

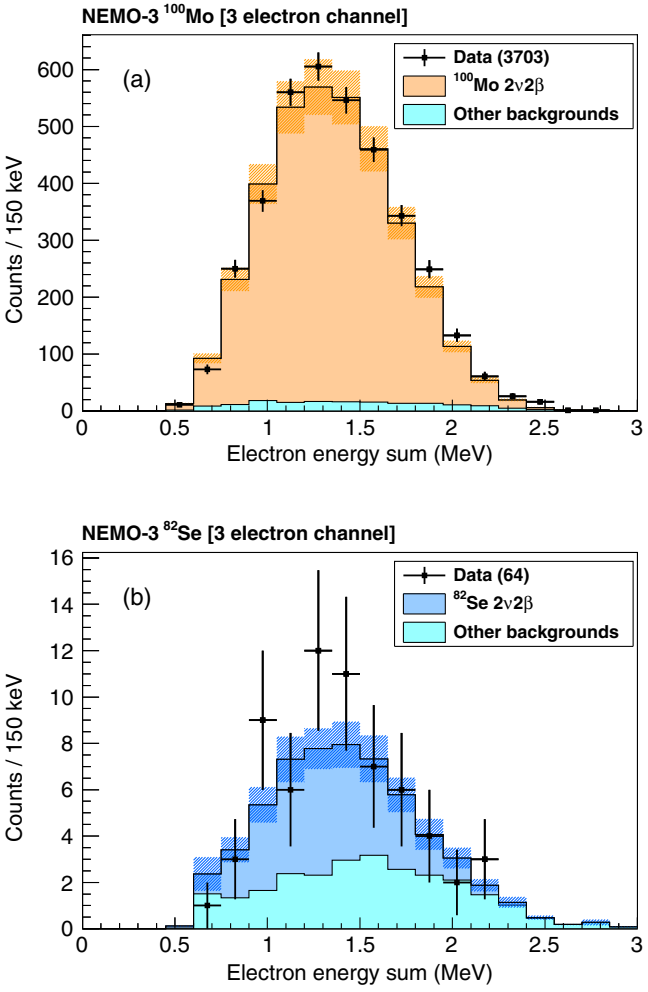

FIG. 2. Energy-sum distributions for three-electron events originating in the source foils of (a) ^{100}Mo and (b) ^{82}Se, which cannot undergo $0\nu4\beta$ decay. The hashed areas represent the systematic uncertainty on the reconstruction efficiency.

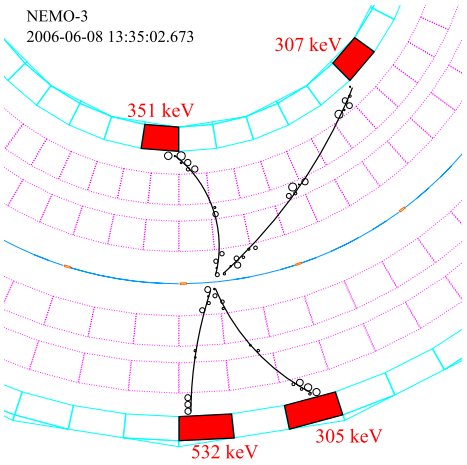

FIG. 3. Display of a decay with four reconstructed electrons in NEMO-3 data, originating in the ^{100}Mo source foil, in the horizontal plane.

time with the electron candidates are rejected, since this would indicate that photons were emitted in the decay.

For the $3e1t$ topology only, we require that there are no delayed hits with times up to 700 μs near the decay vertex or the track end points, caused by an α decay of the ^{214}Po daughter of ^{214}Bi β decays [17]. These decays can occur on the surface of the tracker wires with the β electron scattering in the foil, producing secondaries. The β electron in this type of decay would have no associated calorimeter hit.

To validate the background model, the selection is applied to the foils containing the isotopes ^{100}Mo and ^{82}Se, which are expected to contain no $0\nu4\beta$ signal. The energy-sum distributions for the $3e$ topology, which have higher statistics, are shown in Fig. 2. We observe no events in the $4e$ topology in the ^{82}Se foil, where 0.05 ± 0.01 are expected. We observe two $4e$ candidates in the ^{100}Mo foil, with an expectation of 2.3 ± 0.5 events, of which 2.0 ± 0.4 are due to $2\nu2\beta$ decays followed by double Møller scattering. A display of one of these two data events is shown in Fig. 3.

The total efficiencies for signal decays are shown in Table I and range from 1.81% to 4.61% depending on the kinematic model. The expected background yields are given in Table II for the energy range $1.2 \leq \Sigma E \leq 2.0$ MeV, where ΣE is the electron energy sum, obtained by summing over the calorimeter hits for all reconstructed electrons. All activities and systematic uncertainties, except for the $2\nu2\beta\ 0_1^+$ process, are taken from Ref. [17].

The distributions of the electron energy sum for events originating from the Nd foil are shown in Fig. 4. The energies of the signal distributions are lower than $Q_{4\beta} = 2.084$ MeV due to electron energy losses in the source foil. In addition, only three of the electrons have an associated calorimeter energy measurement for the $3e1t$ candidate events. The distributions show that there are no large differences between the shapes for the different kinematic models.

TABLE I. Signal efficiencies of the four kinematic models for the three topologies.

Topology	Symmetric (%)	Uniform (%)	Semisymmetric (%)	Antisymmetric (%)
$4e$	0.20	0.13	0.04	0.01
$3e$	3.55	3.11	2.39	1.67
$3e1t$	0.86	0.64	0.30	0.13
Total	4.61	3.88	2.73	1.81

We observe no candidate events in the $4e$ and $3e1t$ topologies, with expected background rates of 0.04 ± 0.01 and 0.29 ± 0.05 events, respectively. There is also no significant excess of data in the $3e$ topology, with 22 observed events in the range $1.2 \leq \Sigma E \leq 2.0$ MeV, compared to 16.8 ± 1.7 expected background events.

We consider several sources of systematic uncertainty. The systematic uncertainties on the normalization of the background model given in Table II are the same as those used in Ref. [17], apart from the 25% uncertainty on the half-life of the $2\nu2\beta\,0_1^+$ excited-state decay [19]. The uncertainties of the signal efficiency are given in Table III. The uncertainty on the reconstruction efficiency is determined using the ^{100}Mo data. It is broken down into two independent components, one based on a two-electron efficiency (ϵ_{2e}) uncertainty of 5.5% and the second on a three-electron (ϵ_{3e}) uncertainty of 8.5%. The first value is obtained by comparing the independently measured activity of a ^{207}Bi calibration source with the *in situ* measurements. This uncertainty can only be determined for decays with a maximum of two electrons in the final state. The three-electron uncertainty (ϵ_{3e}) of 8.5% is obtained by comparing the normalization of the $3e$ selection in the simulation and data for the ^{100}Mo foils. This additional uncertainty is applied to both the signal

TABLE II. Expected number of background events for an exposure of 36.6 g × 5.25 yr in the ^{150}Nd source foil in the range $1.2 \leq \Sigma E \leq 2.0$ MeV for the three topologies, with their total systematic uncertainties.

Origin	$4e$ ($\times10^{-2}$)	$3e$	$3e1t$ ($\times10^{-2}$)
^{150}Nd $2\nu2\beta$ (g.s.)	2.08 ± 0.57	9.43 ± 0.84	8.98 ± 0.92
^{150}Nd $2\nu2\beta$ (0_1^+)	0.85 ± 0.36	2.39 ± 0.63	3.98 ± 1.07
^{208}Tl internal	0.74 ± 0.15	1.28 ± 0.21	5.37 ± 1.21
^{214}Bi internal	0.19 ± 0.07	0.74 ± 0.18	1.08 ± 0.30
Other internals		0.82 ± 0.11	1.01 ± 0.51
Neighboring foils		1.61 ± 0.45	1.95 ± 1.91
Radon		0.43 ± 0.15	
Externals		0.12 ± 0.09	6.50 ± 4.12
Total	3.86 ± 0.74	16.8 ± 1.7	28.9 ± 5.4

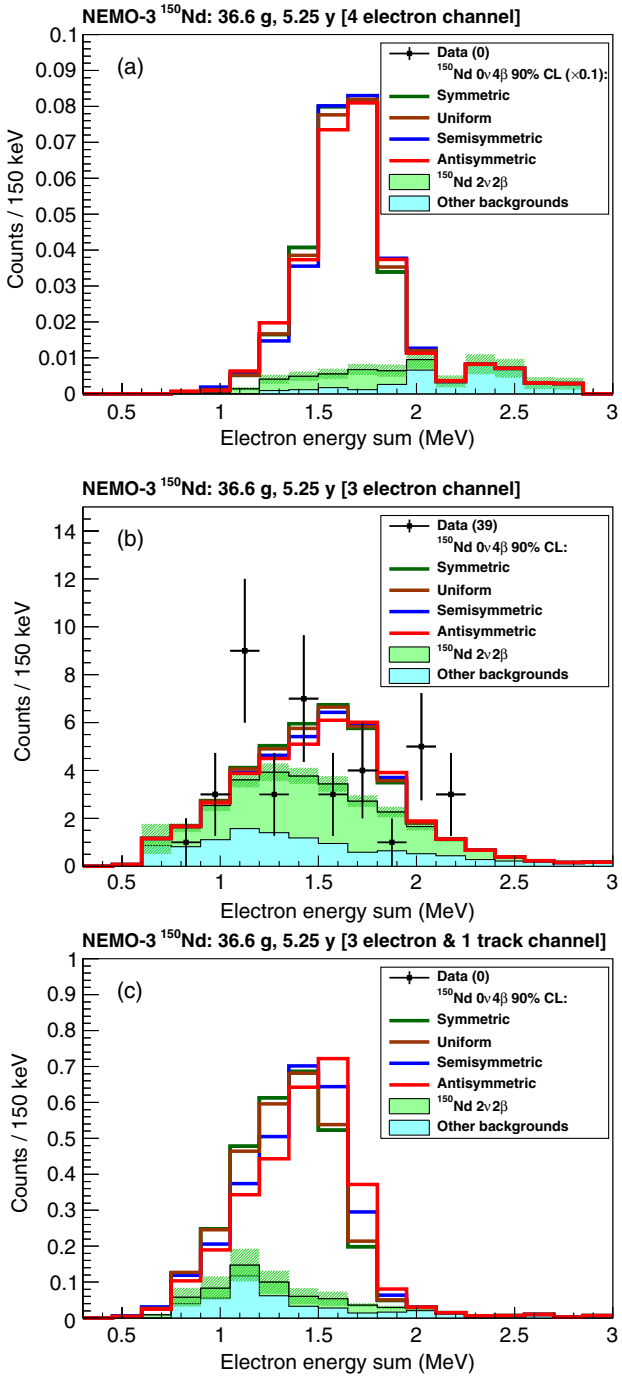

FIG. 4. Energy sum distributions for (a) $4e$, (b) $3e$, and (c) $3e1t$ events in the ^{150}Nd foil for data, the expected background, and signal. The hashed areas represent the uncertainty on the background model. The $0\nu4\beta$ signal distributions are normalized to the 90% C.L. limits, with an additional scaling factor of 0.1 applied to the expected $4e$ signal distributions for better visibility.

efficiency and background models, and is assumed to be the same size in the $4e$ and $3e1t$ topologies. A variation of 2% on the energy scale for all electrons is applied in the simulation to cover uncertainties on the $Q_{4\beta}$ value, the calorimetric energy reconstruction of 0.2% [16], and uncertainties on the simulated energy loss in the foil. We assume an isotropic angular distribution for the electrons from the $0\nu4\beta$ decay. Since the reconstruction efficiency depends on the electron angles, the effect of a different angular distribution needs to be taken into account. We take this systematic uncertainty to be the variance of the reconstruction efficiency over the entire angular range.

TABLE III. Systematic uncertainties on the signal normalization for the three topologies.

Source	$4e$ (%)	$3e$ (%)	$3e1t$ (%)
Reconstruction efficiency (ϵ_{2e})	±5.5	±5.5	±5.5
Reconstruction efficiency (ϵ_{3e})	±8.5	±8.5	±8.5
Energy scale	±12.1	±4.4	±8.5
Angular distribution	±5.7	±1.9	±4.5

For the $4e$ and $3e1t$ topologies, where no candidate events are observed, we set limits using a single bin (with $0<\Sigma E<2$ MeV) for each topology, as for a counting experiment. For the $3e$ topology, we use the binned distribution of Fig. 4(b). Limits at the 90% C.L. are calculated using the modified-frequentist CL_s method [20], which includes the systematic uncertainties with Gaussian priors.

The observed and expected half-life limits $T^{0\nu4\beta}_{1/2}$ are shown in Table IV. We obtain the best sensitivity in the $3e$ topology, due to the much-higher signal efficiency compared to the $4e$ topology. The combined lower limit at the 90% C.L. on the $0\nu4\beta$ half-life is 3.2×10^{21} yr, with a sensitivity, given by the median expected limit, of 3.7×10^{21} yr, assuming a symmetric energy distribution. The combined limits lie in the range $(1.1-3.2)\times10^{21}$ yr for the different models. This result represents the first search for neutrinoless quadruple-β decay in any isotope, and the first search for lepton-number violation by four units.

To improve on this limit in the future using the NEMO-3 technique would not only require more exposure, but also an optimization of the foil density and thickness which causes the main loss of efficiency for low-energy electrons and increases background from Møller scattering. Even with reduced isotope mass, a thinner foil should increase sensitivity.

The authors of Ref. [5] estimate, for their particular model, the ratio R of the $0\nu4\beta$ half-life to the $2\nu2\beta$ half-life to be $R\approx10^{46}(\Lambda_{\rm NP}/{\rm TeV})^4$. For $T^{0\nu4\beta}_{1/2}>1.1\times10^{21}$ yr, this translates to a limit of $R>120$. For $0\nu4\beta$ processes to be observable at the current or future experimental sensitivities, extreme enhancement factors are therefore required. Some possible sources of significant enhancements to the decay rate are discussed in Ref. [5]. This result thus motivates further theoretical and experimental studies of $\Delta L=4$ processes in nuclear decays and at colliders.

TABLE IV. Observed and median expected lower limits at the 90% C.L. on the $0\nu4\beta$ half-life for the four signal models. Systematic uncertainties are taken into account with Gaussian priors.

	Symmetric (10^{21} yr)		Uniform (10^{21} yr)		Semisymmetric (10^{21} yr)		Antisymmetric (10^{21} yr)	
	Observed	Expected	Observed	Expected	Observed	Expected	Observed	Expected
$4e$	0.5	0.3	0.3	0.2	0.1	0.1	0.03	0.02
$3e$	1.6	2.4	1.5	2.1	1.2	1.7	0.9	1.2
$3e1t$	2.0	1.9	1.5	1.4	0.7	0.6	0.3	0.3
Combined	3.2	3.7	2.6	3.0	1.7	2.0	1.1	1.3

The authors would like to thank the staff of the Modane Underground Laboratory for their technical assistance in operating the detector. We thank Werner Rodejohann for useful discussions. We acknowledge support by the funding agencies of the Czech Republic, the National Center for Scientific Research/National Institute of Nuclear and Particle Physics (France), the Russian Foundation for Basic Research (Russia), the Slovak Research and Development Agency, the Science and Technology Facilities Council and the Royal Society (United Kingdom), and the National Science Foundation (United States).

*Corresponding author.
pawel.guzowski@manchester.ac.uk

[1] C. Patrignani *et al.* (Particle Data Group), Chin. Phys. C **40**, 100001 (2016).
[2] J. Schechter and J. W. F. Valle, Phys. Rev. D **25**, 2951 (1982).
[3] R. Arnold *et al.* (NEMO-3 Collaboration), Phys. Rev. D **89**, 111101(R) (2014); J. B. Albert *et al.* (EXO-200 Collaboration), Nature (London) **510**, 229 (2014); K. Alfonso *et al.* (CUORE Collaboration), Phys. Rev. Lett. **115**, 102502 (2015); R. Arnold *et al.* (NEMO-3 Collaboration), Phys. Rev. D **93**, 112008 (2016); A. Gando *et al.* (KamLAND-Zen Collaboration), Phys. Rev. Lett. **117**, 082503 (2016); R. Arnold *et al.* (NEMO-3 Collaboration), Phys. Rev. D **95**, 012007 (2017); M. Agostini *et al.* (GERDA Collaboration), Nature (London) **544**, 47 (2017);
[4] For a recent combination of neutrinoless double-β decay limits, see P. Guzowski, L. Barnes, J. Evans, G. Karagiorgi, N. McCabe, and S. Söldner-Rembold, Phys. Rev. D **92**, 012002 (2015).
[5] J. Heeck and W. Rodejohann, Europhys. Lett. **103**, 32001 (2013).
[6] M.-C. Chen, M. Ratz, C. Staudt, and P. K. S. Vaudrevange, Nucl. Phys. **B866**, 157 (2013).
[7] J. Heeck, Phys. Rev. D **88**, 076004 (2013).
[8] S. C. Chuli, E. Ma, R. Srivastava, and J. W. F. Valle, Phys. Lett. B **767**, 209 (2017).
[9] S. C. Chuli, R. Srivastava, and J. W. F. Valle, Phys. Lett. B **761**, 431 (2016).
[10] M. Nemevšek, F. Nesti, and J. C. Vasquez, J. High Energy Phys. 04 (2017) 114.
[11] M. Wang, G. Audi, F. G. Kondev, W. J. Huang, S. Naimi, and X. Xu, Chin. Phys. C **41**, 030003 (2017).
[12] M. Alanssari, AIP Conf. Proc. **1686**, 020015 (2015).
[13] J. Heeck (private communication).
[14] R. Arnold *et al.*, Eur. Phys. J. C **70**, 927 (2010).
[15] R. Arnold *et al.*, Nucl. Instrum. Methods Phys. Res., Sect. A **536**, 79 (2005).
[16] R. Arnold *et al.*, Phys. Rev. D **92**, 072011 (2015).
[17] R. Arnold *et al.*, Phys. Rev. D **94**, 072003 (2016).
[18] M. F. Kidd, J. H. Esterline, S. W. Finch, and W. Tornow, Phys. Rev. C **90**, 055501 (2014).
[19] A. S. Barabash, Ph. Hubert, A. Nachab, and V. I. Umatov, Phys. Rev. C **79**, 045501 (2009).
[20] T. Junk, Nucl. Instrum. Methods Phys. Res., Sect. A **434**, 435 (1999); A. L. Read, J. Phys. G **28**, 2693 (2002); W. Fisher, Report No. FERMILAB-TM-2386-E, 2007.